Insights into the Hydrodynamics of Free Falling Wavy Films

Three isolated waves of differing amplitude and shape were selected from experimental measurements of a falling liquid film at $Re = 880$ for study using an algorithm developed for solution of the Navier-Stokes equations. The method computes the velocity and pressure fields as well as the velocity of the wave. The results show that large streamwise accelerations exist along with regions of recirculating flow in a moving coordinate system. These features can explain the enhanced rates of heat and mass transfer observed in wavy film flow. Computed wave velocities and wall shear stress were in reasonably good agreement with measurements. Wave velocity is shown to be sensitive to small variations in the wave shape and explains the apparent random variation of wave velocity with amplitude that has been observed experimentally. This numerical experiment points to the shortcomings of the many methods used to model large waves on falling films that have been based on parabolic velocity profiles.

Frederic K. Wasden, A.E. Dukler
Department of Chemical Engineering
University of Houston
Houston, TX 77004

Introduction

Thin liquid films falling under the influence of gravity along solid surfaces are encountered in a wide variety of industrial process equipment, including wetted-wall absorbers, falling-film chemical reactors, condensers, and vertical tube evaporators. Reliable design of these processes depends on the ability to accurately predict the transport rates of heat and mass to the flowing film. At flow-rates of industrial interest, falling films (even in the absence of gas flow) evolve to a highly irregular wavy interface. Figure 1 displays a short time trace of such a falling film. The surface is covered by a complex array of large and small waves moving over a substrate that is less than the mean film thickness. The large waves, which range in amplitude from two to five times the substrate thickness, carry a large fraction of the total mass flowing, and are speculated to control the rate of transport (Dukler, 1977). Before the heat or mass transfer rates to such films can be modeled it will be necessary to understand the velocity distributions that exist within these waves, as well as their evolution. The present work focuses on the former question.

Making reliable experimental measurements of the velocity distribution in the films is exceedingly difficult due to the extremely small film heights ($\approx$1 mm), very short passage time of each wave ($\approx$60 ms) and the random location of the wave height, as seen in Figure 1. Nonintrusive methods such as LDA (Laser Doppler Annenometer) do not provide sufficiently fine resolution to investigate velocity profiles. Thus, experimental measurements appear limited to the time variation of wall shear stress and film thickness. As a result, analytical models have been developed in the absence of hard data on the true flow conditions that appear to exist in the waves.

Most analytical models extend the concepts advanced by Kapitza (1964) based on the use of a parabolic velocity profile and assuming that the streamwise hydrodynamic variables scale with the wavelength. In examining various models developed to that date, Dukler (1972) concluded that all failed to accurately represent any measured characteristics of the wave except at Reynolds numbers well below those of industrial interest.

Maron et al. (1985) treated isolated waves as a series of segments, each having a different type of velocity distribution depending on the physics of the region. In the substrate, a parabolic velocity profile was adequate, while the flow under the front of the wave was assumed to be fully mixed. The slowly varying wave back was described with a boundary layer model. Upon matching these solutions at the segment boundaries, it was possible to predict wave mean characteristics (height, length, velocity, substrate thickness) in reasonable agreement with the values measured by Zabaras (1985). The model was fitted with a limited amount of data from experimental measurements and it failed to explain the large variation observed in individual wave amplitudes and lengths.

Modeling the wavy film flow by a direct solution of the Navier-Stokes equations is hampered by numerical stiffness imposed by the stress-free interface; as a result, convergence is difficult except at the lowest flow rates. Bach and Villadsen (1984) explored the application of a finite-element scheme to the unsteady problem of waves developing from initial perturbations

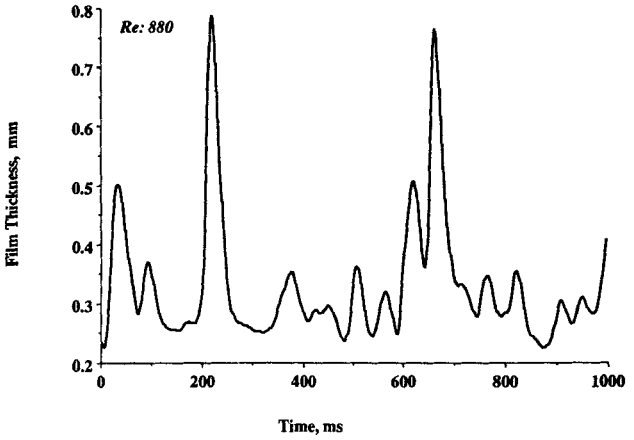

Figure 1. Film thickness time trace.

on the smooth film for Reynolds numbers up to 100. Their work predicted that the equilibrium condition would consist of waves having one general shape, a condition contrary to experimental fact even at film Reynolds numbers as low as 1. The film Reynolds number is defined as $Re = 4\,Q/\nu$, where Q is the mass flow rate per unit perimeter, and ν is the kinematic fluid viscosity. Kheshgi and Scriven (1987) applied a finite-element technique to a problem with periodic boundary conditions in the flow direction, and verified the evolution of infinitesimal disturbances as predicted by Orr-Sommerfeld analyses. Their work was limited to low flow rates, and failed to generate waveforms comparable to those observed experimentally for fully developed flow.

In the absence of analytical models for velocity profiles that appear to represent reality, and due to the absence of suitable experimental methods for measuring these profiles, a series of numerical experiments were undertaken. Wave shapes, wall shear stress profiles, and wave velocities were measured in our laboratory for a film Reynolds number of 880, chosen to insure significant inertial forces while remaining viscous in nature. A novel method of solving free surface flows was developed, using experimentally determined film thickness data for large, isolated waves to solve for the position of the free interface. The results of these computations demonstrate the complex dependence of velocity distributions on wave shape, and represent an early step toward realistic modeling of large waves.

Experimental Procedure

Flow loop

For fully developed wavy film flow, film thickness and wall shear stress data were collected in a 50.8 mm ID vertical test section in a flow loop described by Zabaras et al. (1986). After being pumped through a calibrated rotameter, the aqueous solution entered the column through an annulus whose inner wall consists of a stainless steel porous sinter having 100 μm pore size. Combined with careful leveling of the column prior to data collection, this entry section insured minimal deviations from axisymmetric flow and produced a smooth inlet flow. The measuring station was located 3.1 m below this entry section.

Measuring station and measurement techniques

The measuring station, shown in Figure 2, is patterned after that described by Zabaras et al. The removable section allows

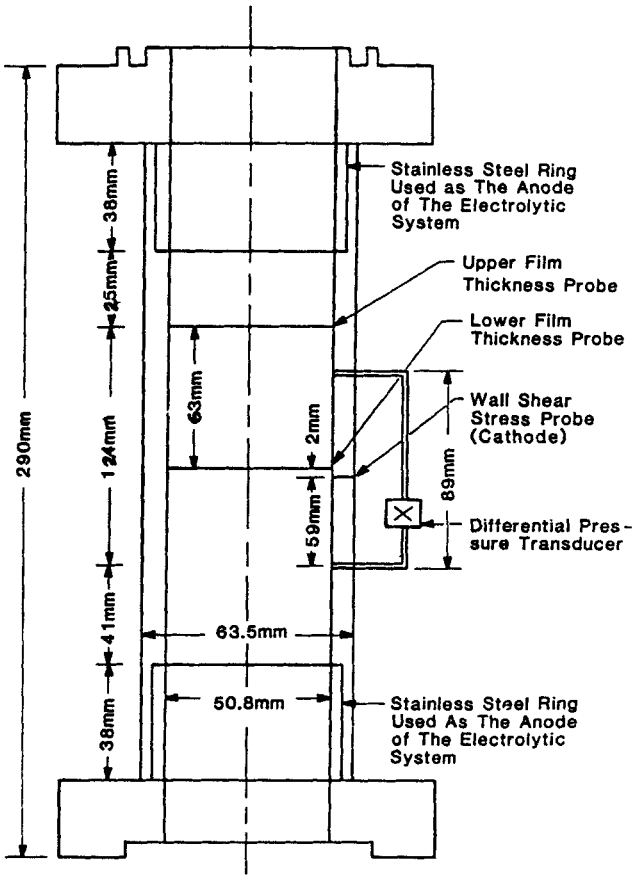

Figure 2. Measuring station.

simultaneous measurement of film thickness and wall shear stress at one location and of thickness at another. The station was constructed of the same material as the flow loop, and was carefully machined to insure a smooth transition to the station.

Film thickness probes consisted of twin parallel platinum-13% rhodium wires of 0.05 mm dia., spaced 2.5 mm apart, which penetrated the flow. As described in detail by Brown et al., (1978), a linear relation exists between the resistance of the film between the wires and the film thickness. Calibration proceeded by setting the measuring station horizontal, blocking the ends, and introducing different fluid levels, determined to within 10 μm by using a cathetometer, followed by measurement of the resulting resistance. Downstream electronics for converting this resistance to a DC voltage signal are described elsewhere (Zabaras et al., 1986). Conductance of the fluid was monitored closely at all times during the calibration and data collection procedures to insure proper correction of any thermally induced conductance drift.

Wall shear stress measurements were based on the electrochemical mass transfer method described by Hanratty and Campbell (1983). For the present series of measurements, the iodine/tri-iodide system was chosen. The working solution contained 0.1M KI and 0.004M I_2(s) in demineralized water, and was replaced every 2 h to minimize errors due to iodine evaporation. A dry nitrogen atmosphere was used in the flow loop to minimize oxygen saturation of the solution. Fluid properties at 25°C are: density, 1,010 kg/m^3; absolute viscosity, 8.50×10^{-4} kg/m · s; and surface tension, 7.12×10^{-2} N/m. The cathode

for this system consists of a flush-mounted strip of platinum foil, 0.075 mm (in the flow direction) by 1 mm wide, embedded in Plexiglas to insure electrical isolation. By measuring the current produced by an electrochemical reaction at the surface of the cathode, the wall shear stress at that location is determined. For the redox reaction

$$I_3^- + 2e \rightarrow 3I^- \qquad \text{(cathode)}$$
$$3I^- \rightarrow I_3^- + 2e \qquad \text{(anode)}$$

a concentration boundary layer develops on the cathode surface, which is polarized at -0.8 VDC to insure the concentration approaches zero. For the iodine system, the range of polarization voltage is quite broad, insuring that large increases in flow rate will not deplete the electron source at the cathode. Details concerning the downstream electronics and calibration associated with this measurement technique are found elsewhere (Zabaras et al., 1986).

It is now recognized (Mao and Hanratty, 1985) that the response of the electrochemical probe is highly dependent on the nature of the "input" wall shear stress. For the ionic system employed in this study, errors in both phase and magnitude are expected to be small due to the large ($10^3\ s^{-1}$) mean velocity gradient, small cathode surface area, and large Schmidt number (ν/D) of the fluid ($\approx$780). The relationship given by Hanratty and Campbell (1982) between cathode current and wall shear stress was used in this study, as the frequencies in the data were sufficiently low to allow the use of a quasi-steady analysis.

Data collection, processing, and analysis

Voltage signals from two film thickness probes and the wall shear stress probe were first low-pass filtered at 1 kHz, then fed to a microcomputer-based analog to digital (A/D) converter. Each signal was digitized at 1 kHz by a Data Translation 12 bit A/D converter installed in a DEC Micro 11/73 microcomputer. The data set comprised 1 min of data, and was stored on the system Winchester disk prior to applying calibration curves and writing the data to magnetic tape for further analysis. Digitization and collection errors are expected to be negligible for all data, while calibration errors for the film thickness measurement are expected to be less than 3%. Errors inherent in applying steady state wall shear stress calibration curves depend on the nature of the input signal, requiring separate examination of individual results. Zabaras (1985) reports estimated errors of less than 7% for this technique.

Film thickness and wall shear stress data was examined to locate isolated waves, defined by a wave having a peak to substrate thickness ratio greater than 2, and surrounded by at least one wavelength of reasonably flat film. For the sequences of raw data, three representative waves of various dimensions were chosen for computational domains. For each case, a nominal wave velocity was determined from the time necessary for the wave to travel from the upper to lower film thickness probes.

Numerical Method

Solution of free-boundary problems requires methods for both the solution of the governing momentum equations and shape determination. The velocity and pressure fields within the wave were determined by solving the Navier-Stokes equations in primitive variable form. For a film Reynolds number of 880, the wave thickness generally was less than 1% of the pipe radius, and therefore a two-dimensional Cartesian coordinate system was chosen. The transformation of time traces of film thickness to this coordinate system comprised the shape determination portion of the overall algorithm. The common method of computing the position of a free interface, $h(x)$, is to determine the value of the film thickness, h, at given values of the streamwise variable, x. The present method inverts the process: for given, measured values of h, we find the values of x that result in $h(x)$ satisfying all of the free interface boundary conditions. To insure accurate representation of the interfacial pressure, a fourth-order-accurate, divided-differences scheme was used to compute the curvature of the interface:

$$h_{tt}/(1 + h_t^2)^{3/2} \tag{1}$$

Initially, the waves were modeled as though their shape remained constant with time; these waves are termed "solitary." The new streamwise coordinate, z, is fixed on the wave, and originated at the front of the wave. The film thickness profile in the time domain, $h(t_i)$, was converted to the length domain, $h(z_i)$, through the transformation

$$z_i = z_o + V_w(t_i - t_o) \tag{2}$$

for i ranging from 1 to the number of film thickness points in the isolated wave. In this manner, the wave profile was "stretched" for use as a computational domain, and time was removed from the problem. For this coordinate system, the wave remains fixed, and the wall moves upward at a constant speed given by V_w, the wave velocity for the solitary wave.

It is useful to define a new streamwise velocity component,

$$u(z, y) = u'(x, y) + V_w, \tag{3}$$

where $u'(x, y)$ is the streamwise velocity in a coordinate system fixed on the wall. The governing equations for this viscous, incompressible, and isothermal flow relative to the moving wave become

$$uu_z + vu_y = -P_z/\rho + \nu\Delta u + g \tag{4}$$

$$uv_z + vv_y = -P_y/\rho + \nu\Delta v \tag{5}$$

$$u_z + v_y = 0 \tag{6}$$

where v is the velocity in the normal (y) direction, P is the pressure, g represents gravitational acceleration, and ν and ρ are the kinematic viscosity and density of the fluid, respectively. At the stress-free interface, $y = h(z)$, tangential and normal stress balances require

$$(u_y + v_z)(1 - h_z^2) - 2h_z(u_z - v_y) = 0 \tag{7}$$

$$P = \sigma h_{zz}/(1 + h_z^2)^{3/2} + [2\mu/(1 + h_z^2)]\,[u_z h_z^2 - (u_y + v_z)h_z + v_y] \tag{8}$$

where σ is the surface tension coefficient. At the wall, $y = 0$,

$$u = V_w, \qquad v = 0, \tag{9}$$

represent the standard no slip and no flux conditions. Velocities at the interface are related through the kinematic condition in a moving frame,

$$v = uh_z, \qquad y = h(z). \tag{10}$$

The inlet velocity profile is parabolic, representing an acceleration-free falling film, while a sufficient and physically consistent outlet condition for a solitary wave requires a zero streamwise derivative for all variables. The variable V_w replaced $h(z)$ as the final variable to be iteratively determined in the free-surface problem, and completes a now well-posed problem.

For each wave profile, a unique, nonuniform finite-difference grid mesh was constructed. The mesh for a typical domain is shown in Figure 3. The particular wave shape determined the grid spacing used. Mesh refinement continued until no further change in either the computed wave velocity or wall shear stress profile was observed. Of particular importance was the concentration of cells near the front and top of the wave, since the velocity fields change drastically in this region due to the large interfacial slope and curvature. For most waves, 1,200 cells of dimension $\delta x \delta y$ were sufficient, and produced grid Reynolds numbers [$Re_{Gx} = u(z, y)\,\delta x/\nu$, $Re_{Gy} = v(z, y)\,\delta y/\nu$] of order 1 in the y direction, and ranging from 1 to 100 in the streamwise direction.

The curved interface was accommodated by allowing boundary cells to be cut by the boundary, $h(z)$, thus reducing their volume. This situation is illustrated in Figure 4. This technique produced areas adjoining two boundary cells, the centers of which were outside the computational domain. As the stress-free interface requires a zero normal derivative of the velocity vector with respect to the boundary, $h(z)$, these regions were treated as inviscid channels through which all fluid leaving one boundary cell on its shared side passed into the neighboring cell through its respective shared side. The total area of these regions represents less than 0.1% of the total domain, and had little effect on the results.

The equation set was solved on a finite-difference grid using a variant of the TEACH-T code (Gosman et al., 1969), incorporating the SIMPLER pressure-continuity solution procedure; the principles of this method are described in detail elsewhere (Patankar, 1980). The domain includes regions of significant streamwise variation in all variables, thus necessitating an accurate method of discretizing convective momentum terms. The simplest method of convective discretization, upwind differencing insures a reasonably stable numerical solution, but introduces numerical diffusion in regions of the flow where streamlines are oblique with respect to the grid lines (Raithby, 1976). More importantly, the upwide scheme lacks sensitivity to cross-stream diffusion and source terms (Leonard, 1979), which are of tremendous importance in the case of a thin film. This lack of sensitivity diminishes the effects of the y direction diffusion as well as the v velocity in the solution of the streamwise velocity. These deficiencies in the upwind and hybrid methods require the use of a QUICK-based scheme, which improves accuracy by expanding the number of neighboring points included in interpolated values of velocity.

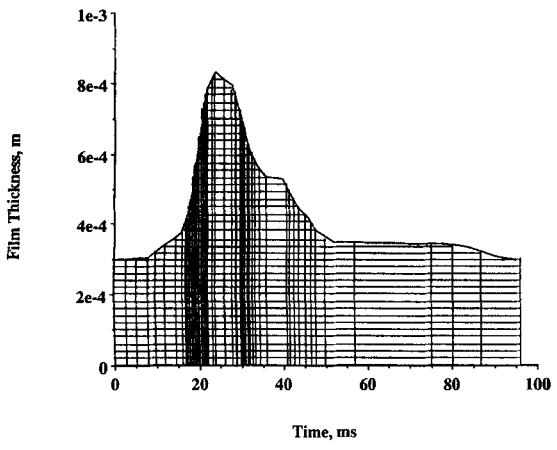

Figure 3. Sample finite-difference grid.

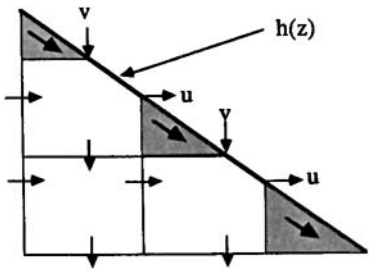

Figure 4. Interface finite-difference grid.

Based on Leonard's (1979) third-order-accurate discretization scheme QUICK, Pollard and Siu (1982) developed the QUICK-ER (Extended and Revised) method of discretizing convective terms. The QUICK-ER method overcomes stability problems inherent in the QUICK procedure at the expense of slower convergence, and is considered the most satisfactory method of handling convective momentum terms (Huang et al., 1985). For application to nonuniform grids, a new version of QUICK-ER was developed. This method follows the spirit of the QUICK-ER formulation, but includes locally variable weighting factors to account for the nonuniformity of the grid in both directions. Although QUICK-ER schemes requires more computational effort per iteration than upwinding, particularly for nonuniform grids, improvements in accuracy allow the use of a slightly coarser grid, so total computational time exceeds that required by the upwind method by only 20%.

The solution procedure began with choosing a value for V_w and creating the transformed domain, given by Eq. 2. The u velocity field was set to a parabolic profile everywhere, and the v velocity field was set to zero. The pressure at each z location was set to the surface pressure due to curvature. Updated velocity and pressure fields within the wave were then computed using Eqs. 4, 5, and 6. Through interpolation for the velocity gradients in the interfacial shear stress balance, Eq. 7, streamwise and normal velocities in the interior of the flow field were used to derive an expression for the streamwise surface velocity. Coupled with the kinematic condition, Eq. 10, the velocities on the surface were known for each iteration. The surface pressure computed from Eq. 8 was used to determine the first pressure value in the interior of the domain through the use of parabolic interpolation using the surface pressure and two interior pressures. With the newly computed surface variables, the velocity and pressure fields were updated until the sum of residuals of mass and momentum (normalized by the inlet quantities) over the domain was less than 10^{-3}. This condition also required the

interfacial shear and normal stress balances to be within 10^{-2} Pa of zero, and thus, the governing equations and boundary conditions were satisfied.

Upon convergence of the velocity and pressure fields, the average pressure in the flat outlet section was examined. If the average pressure did not approach zero, as required for a nonaccelerating film surrounding a solitary wave, a new value of V_w was chosen and the process repeated. The adjustment procedure for V_w was simple: If the pressure in the outlet section was higher than zero, the wave (wall) velocity was too high, since the wall was pushing excess fluid through the wave, and a positive pressure at the outlet was opposing this extra fluid in an attempt to satisfy the mass balance for the wave.

Examination of the experimental data reveals that the large waves do not remain precisely constant in shape. Incorporating this unsteady effect is accomplished through the use of a locally constant stretching parameter, as opposed to the globally constant value used for the classical solitary wave. The domain transformation for this case is given by:

$$z_i = z_o + V_{wi}(t_i - t_o) \tag{11}$$

where z is the streamwise coordinate. In general, this pseudo-wave velocity is

$$V_{wi} = V_w\,[1 - e(z_i)] \tag{12}$$

where $e(z_i)$ is an iteratively determined local stretching variable, and V_w represents the wave velocity associated with the substrate. The solitary wave case is recovered by setting $e(z_i) = 0$ for all i. As before, we define a new streamwise velocity component as

$$u(z, y) = u'(x, y) + V_w(z_i) \tag{13}$$

which allows the same governing equations and boundary conditions, Eq. 4–10, to apply, The transformation, Eq. 12, introduces a locally variable mass and momentum source due to the evolving nature of the wave, which does not appear in a solitary wave. The solution procedure is identical to that of the purely solitary wave. The solution procedure is identical to that of the purely solitary wave, with the exception that now a profile of V_{wi} must be specified instead of a single value. When the velocity and pressure fields have converged for a given set of V_{wi}, the wave shape is adjusted through $e(z_i)$ to meet two criteria. The baseline wave velocity, V_w, was adjusted such that the average pressure in the flat outlet section approached zero, as before. The computed wall shear stress profile was then compared to the experimental profile, and adjustments made to $e(z_i)$ to correct deviations. In this sense, the classical free-boundary problem is recovered, albeit supplemented by experimental data.

The procedure developed for the solitary waves required an average of 300 iterations of the velocity and pressure fields to converge, with an underrelaxation factor of 0.5 used for all variables. Between four and eight adjustments to the solitary wave velocity were required to produce a flow with an average outlet pressure less than 10^{-2} Pa. For the quasi-unsteady case, the same number of iterations was required to achieve convergence of the velocity and pressure fields, while the adjustment of the variable wave velocity to match wall shear stress data took anywhere from five to 20 iterations.

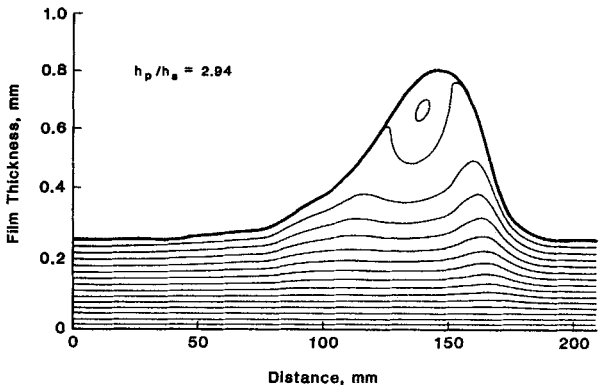

Figure 5. Solitary wave streamline map, peak/substrate ≈3.

The program was coded in FORTRAN 77, and required 2 MB of task space. Execution times for convergence of the velocity and pressure fields were approximately 5 CPU h on a VAX 11-750 computer.

Results

Initial computations explored the validity of neglecting the evolution of the wave shape. For a peak/substrate thickness ratio of approximately 3, the resulting streamline map and wall shear stress profile comparisons are shown in Figures 5 and 6. The body force due to gravity, ρgh, is presented to accommodate comparison with the wall shear stress predicted by a parabolic velocity profile. The shear stress comparison suggests that the front and back of the wave are accurately described as moving undeformed, but neglecting the evolution of the peak of the wave causes discrepancies between computed and measured wall shear stresses. Figure 7 shows superposed traces of the film thickness measured at locations 63 mm apart, and clearly illustrates the slight difference in speed between the front and back of the wave as it moves down the tube, suggesting $e(z_i) > 0$ in this front region. In order to evaluate the effect of small changes in velocity along the wave, the parameter $e(z_i)$, given by Eq. 12, was varied by trial and the effect on the resulting wall shear stress comparison noted. Figure 8 shows the very slight degree of

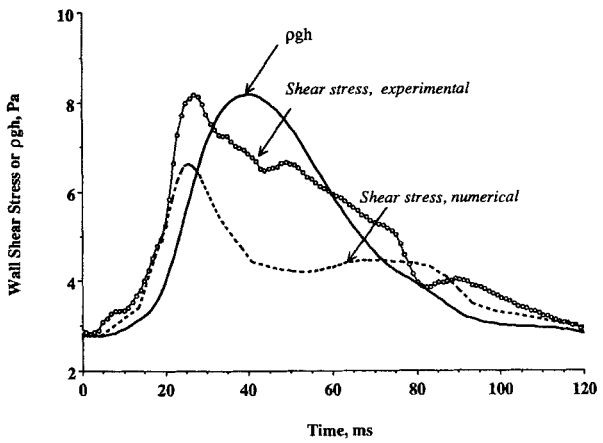

Figure 6. Solitary wave shear stress comparison, peak/substrate ≈3.

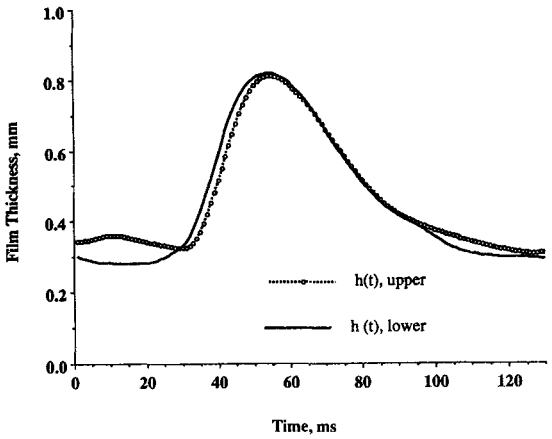

Figure 7. Evolution of nearly solitary wave, peak/substrate ≈3.

variation in V_w along the front of the wave, which resulted in satisfactory agreement between measured and computed wall shear stress data along the wave. To accomplish this match, the wave velocity was increased gradually over the front of the wave, reaching a maximum deviation of roughly 10% directly under the peak. The effect of this variation on the streamlines and shape of the domain is small, but still significant, as seen in comparing Figure 9 with Figure 6. While the flow near the wall appears quite sensitive to unsteady effects, global flow patterns show only small sensitivity to these changes. These results emphasize the importance of the interfacial shape in the computation of the flow field.

Streamline maps of two additional waves, having peak/substrate thicknesses of approximately 4 and 5, are presented in Figures 10 and 11. Streamlines for these larger waves were less affected by the transition from solitary to evolving waves than the smaller wave. For these larger waves, the $e(z_t)$ factors were slightly larger than in the previous wave, and the wall shear stress comparisons were similarly favorable. These streamline maps, in conjunction with Figure 9, suggest it is reasonable to view the waves as lumps of fluid overrunning a slow moving substrate. Note that for all three of these waves of different amplitude, a well-defined recirculatory region appears when viewed in

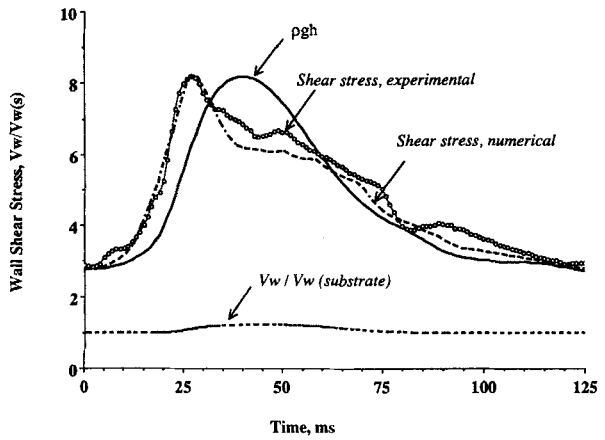

Figure 8. Shear stress comparison for evolving wave, peak/substrate ≈3.

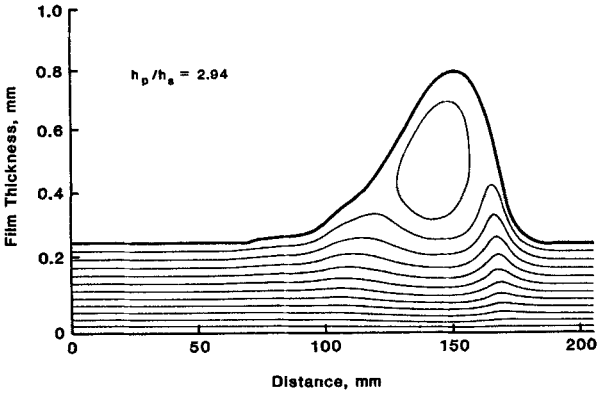

Figure 9. Streamline map for evolving wave, peak/substrate ≈3.

a coordinate system fixed on the wave. Of importance is the presence of large normal velocities near the front and rear of the recirculating region. Previous modeling characterized all normal velocities as small corrections to the dominant streamwise flow, a supposition now seen to be inaccurate. These normal velocities can be expected to enhance transport by refreshing the surface with fluid from the substrate.

Surface velocity of the waves is nearly uniform over a large portion of the wave peak, while varying rapidly near the front. Note the presence of stagnation points in front of and behind each wave peak. While not physically important features of the flow, these points correspond to zero curvature of the streamwise velocity, and are unrealizable for a parabolic velocity profile.

Most previous modeling efforts have regarded acceleration within the wave as negligible compared to the gravitational acceleration. In the Kapitza, or long-wave, analysis, the inertial terms are neglected to produce a linear hydrodynamic problem, which yields the streamwise velocity

$$u(z, y) = (g/\nu)\,[yh(z) - y^2/2] \tag{14}$$

For this simple velocity profile, it is easily shown that the inertial forces, normalized with respect to gravity, are

$$(u\partial u/\partial z + v\partial u/\partial y)/g = (g/\nu^2)y^2h(z)/2(dh/dz) \tag{15}$$

which has a maximum value at the interface, $y = h(z)$, given

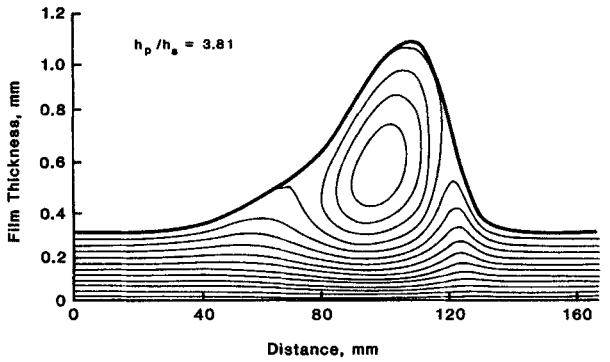

Figure 10. Streamline map for evolving wave, peak/substrate ≈4.

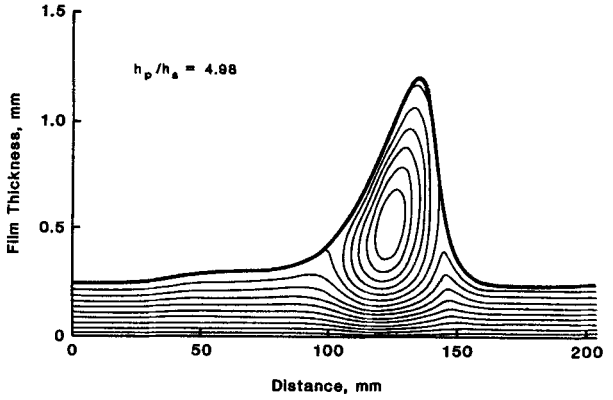

Figure 11. Streamline map for evolving wave, peak/substrate ≈5.

by

$$gh(z)^3(dh/dz)/(2\nu^2) \tag{16}$$

Using the physical properties given previously, this quantity (for $Re = 880$) becomes $O(10^2)$ dh/dz. For the original linearization of the problem to be valid, Eq. 16 suggests dh/dz should be less than $O(10^{-3})$. The large waves discussed here have slopes as great as 0.07, in which case inertial forces are predicted to dominate gravity, and the original premise is violated. Further comparison of the computed inertial forces and the long wave predictions, Eqs. 15–16, must be limited to the location of extrema and existence of inertial forces when the interfacial slope is small.

As seen in the streamline maps, large accelerations exist near the surface, particularly near the front and rear of the recirculating region. For the wave having a peak/substrate thickness ratio of roughly 3 (a ratio commonly seen in experimental data), consider the three locations shown in Figure 12. Near the front of the wave, maximum normalized inertial forces (convective momentum terms/gravity), shown in Figure 13, are several times greater than gravity. Beneath the wave peak, roughly 25% of the flow is free of acceleration, a stagnant lump riding on the substrate. In this region, the interfacial slope is nearly zero, for which Eq. 16 predicts no acceleration whatsoever. However, the

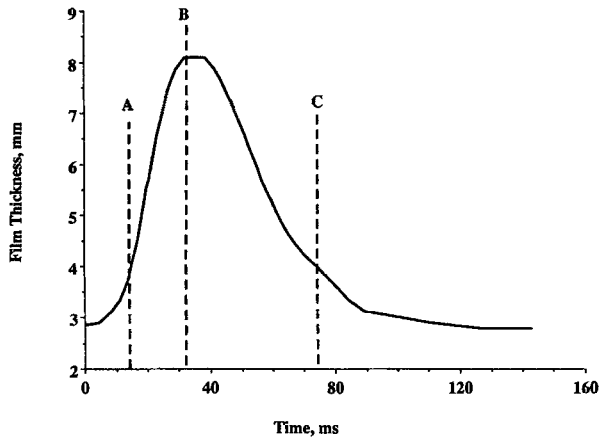

Figure 12. Location of acceleration and velocity fit examples, peak/substrate ≈3.

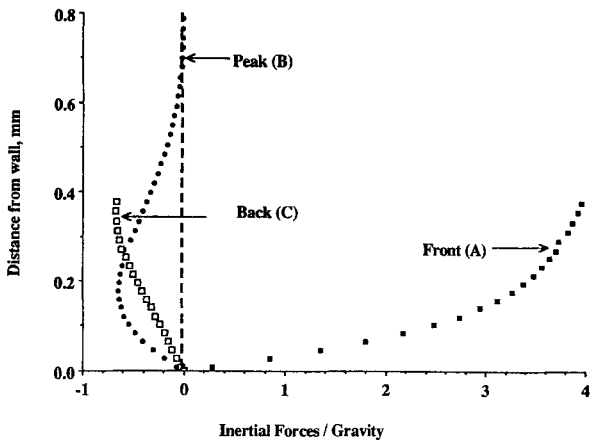

Figure 13. Convective acceleration profile, peak/substrate ≈3.

substrate beneath the peak shows moderate deceleration, with the maximum occurring far from the interface, contradicting Eq. 15, which requires the maximum inertial force to exist at the free interface. Further toward the back of the wave, the acceleration is again maximum at the surface, showing a deceleration of the order of gravity, while Eq. 16 predicts a maximum acceleration of the order of 10^{-1} g for this nearly flat region. These variations in acceleration in the streamwise direction support the premise of large waves pushing material from the surface to the substrate, exchanging either heat or mass, and thereby enhancing transport properties.

Acceleration effects are further illustrated in Figure 14; a particle on a surface streamline would undergo greater changes in acceleration than one near the wall. The process of transport enhancement is again clearly shown, as particles in front of the peak accelerate toward the mass of stagnant fluid, exchanging heat or mass, and then are forced to return to the substrate.

To examine the suitability of various polynomial representations of the streamwise velocity profile, data from the numerical experiment were compared to the velocity profile predicted by Kapitza analysis,

$$u(z, y) = 2u[z, y = h(z)]\,\{y/h(z) - \tfrac{1}{2}\,[y/h(z)]^2\} \tag{17}$$

where the surface velocity was taken from the numerical experiment. In addition, the computed velocity profile was fit with a least-squares cubic polynomial in y. For illustrative purposes, consider the streamwise locations within the wave shown in Figure 12. Near the front and beneath the peak, the parabolic fits

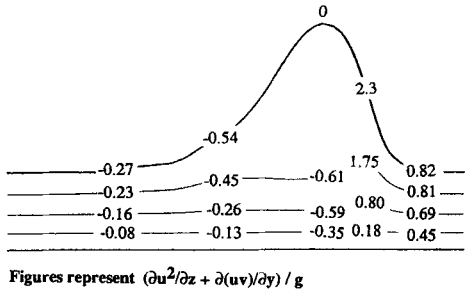

Figure 14. Fluid particle acceleration, peak/substrate ≈3.

shown in Figures 15a and 15b show significant deviations from the computed velocities, while the cubic polynomial appears to faithfully represent the profile. Use of the cubic polynomial allows the curve to fit the velocity gradient at the wall as well as the surface and wall velocity accommodated by the parabolic fit. This extra degree of freedom enables a nearly perfect fit of the data, and represents the physically desirable property of matching wall shear stress as well as surface velocity. Near the back of the wave, where the shear stress suggests the flow has small acceleration forces, the cubic and parabolic fits are shown in Figure 15c to coincide more closely than at other locations.

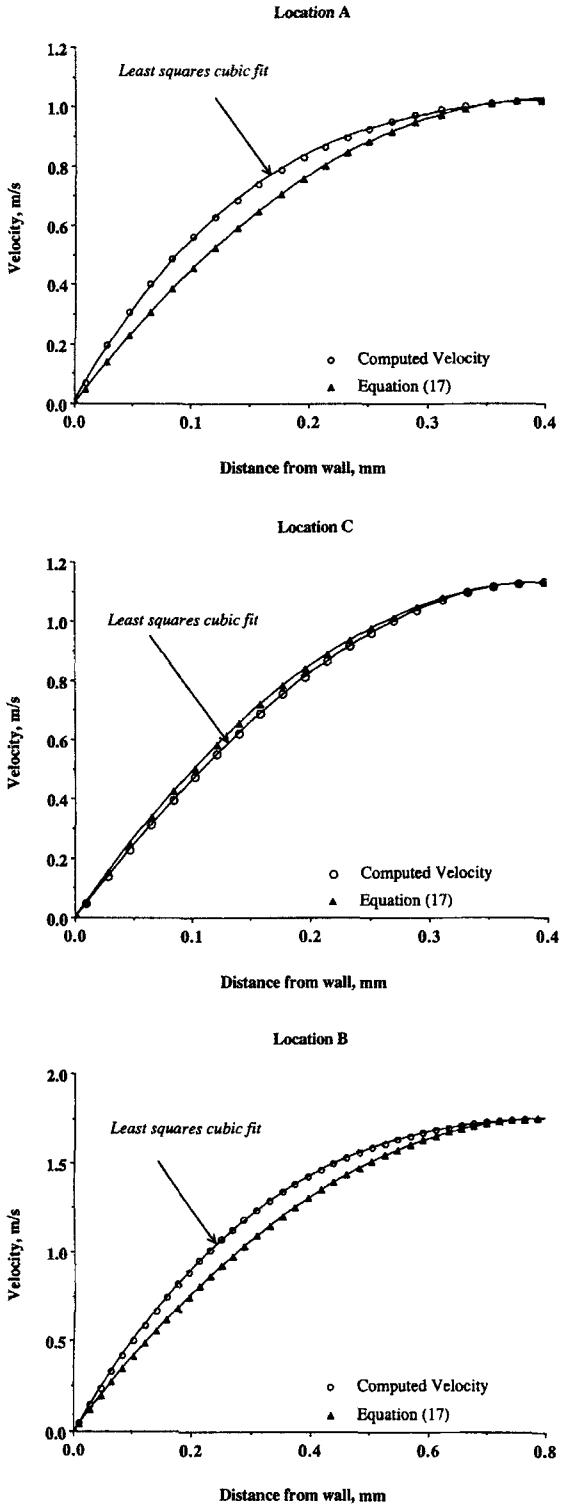

Figure 15. Curve fits of velocity profiles, peak/substrate ≈3.

In the cases of both solitary and evolving waves, the wave velocity V_w was computed by choosing V_w such that the average outlet pressure was close to zero. The dependence of average outlet pressure on the wave velocity is shown in Figure 16 for the solitary wave with a peak/substrate ratio of approximately three. This nearly linear dependence allowed quick convergence to V_w. For each wave, the substrate or base wave velocity V_w was compared to that determined by dividing the length between the upper and lower film thickness probes by the passage time of the wave peak. In cases where the wave traveled between the probes with only slight deformation, this comparison showed the computed values to be within roughly 10% of the experimental ones. For those waves evolving rapidly, this crude comparison produced less favorable results, with errors as high as 30% for the wave and peak/substrate of approximately 5.

Figure 17 shows the values of non-dimensional wave velocity determined by simulating flow in various solitary waves at different flow rates. The hydrodynamic character of these waves was similar to those presented in detail: of primary interest was the lack of correlation of wave velocity to peak/substrate thickness, in agreement with the experimental findings of Zabaras (1985).

Conclusions

The interface of a falling liquid film consists of a random array of waves of varying amplitude, length, and velocity, some isolated and some overlapping. Even at moderate Reynolds numbers, these waves display amplitudes that are two to five times the substrate thickness. Three typical isolated waves obtained from measurements of the time traces of the film thickness were selected as computational domains. A method was developed to solve the Navier-Stokes equations for this free-surface problem which yields both velocity and pressure fields in the wave and wave velocity. The measured wall shear stresses and wave velocities were in reasonable agreement with those determined from the numerical solutions. The results of these computations confirm certain earlier speculations on the me-

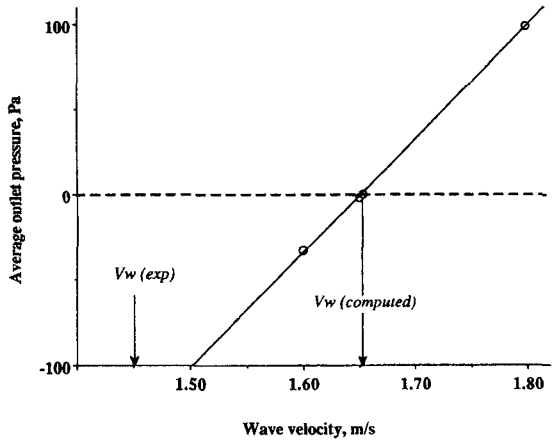

Figure 16. Average outlet pressure dependence of wave velocity, peak/substrate ≈3.

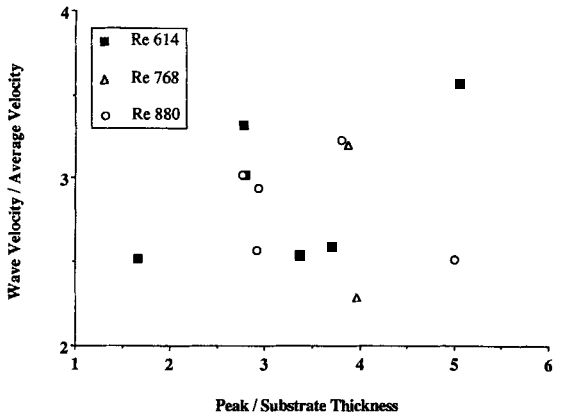

Figure 17. Numerical predictions of wave velocity.

chanics of wavy film flow and point to the inadequacies of others.

The large wave moves rapidly over a slow substrate, the bulk of the liquid being carried in the wave; this liquid is nearly stationary in a coordinate system moving with the wave. The interaction between the wave and substrate causes the acceleration of fluid at the front of the wave from the substrate in the peak. The fluid then decelerates as it passes out the wave back, generating a close recirculation region in the wave whose size depends on the wave amplitude. This process of recirculation would appear to account for the enhanced rates of heat and mass transfer known to exist in wavy films. This picture of the waves is in rough accord with the speculations of Dukler (1977).

The presence of secondary flows can be expected to enhance rates of interfacial mass transfer. Levich (1962) showed that velocities normal to wall as small as 1% of the streamwise velocity produces a 15% increase in the rate of mass transfer to the interface. As the present work shows that normal velocities may be ten times this large, we expect substantial enhancement.

Most previous studies of wavy film flows, starting with the classical work of Kapitza (1964), are based on the parabolic streamwise velocity profile, which is presumed to exist at all positions along the wave. This numerical experiment points to the inadequacy of that assumption for these large waves, and shows that a cubic profile faithfully reproduces the streamwise velocity gradient at all axial locations. Attempts to develop evolutionary equations for this flow should use the higher order velocity profile to insure that the accelerations which exist can be incorporated into the model.

Most theoretical models have shown that the wave velocity and amplitude are uniquely related. Careful measurements by Zabaras (1985) show that the wave amplitude varies widely with both amplitude and wave length. These numerical studies show that for a given amplitude, the computed wave velocity is sensitive to relatively small changes in wave shape, rationalizing the experimental observations and raising questions as to the usefulness of some of the simpler models.

The use of a single wavelength as a scaling parameter for the streamwise hydrodynamics is shown to be incorrect. The present computations show that strong differences in accelerations exist at various positions along the wave. Each of these domains should be analyzed separately if integral equations are to be used, as suggested by Maron et al. (1985). The use of evolutionary equations can eliminate this problem.

Acknowledgment

Financial support of this research by the Office of Naval Research is gratefully acknowledged. F. K. Wasden was supported by a National Science Foundation Graduate Fellowship.

Notation

D = liquid -liquid diffusion coefficient, m^2/s
g = acceleration of gravity, m/s^2
P = pressure, N/m^2
Q = liquid film flow rate per unit perimeter, m^2/s
Re = film Reynolds number, $4Q/\nu$
Sc = Schmidt number, ν/D
u = local streamwise velocity, m/s
v = local velocity normal to boundary, m/s
V_w = solitary wave velocity, m/s
x = axial coordinate in lab frame, m
y = coordinate normal to boundary, m
z = coordinate fixed on wave, m
ρ = liquid density, kg/m^3
ν = liquid kinematic viscosity, m^2/s
Δ = Laplacian operator, $\partial^2/\partial x^2 + \partial^2/\partial y^2$

Literature Cited

Bach, P., and J. Villadsen, "Simulation of the Vertical Flow of a Thin, Wavy Film Using a Finite-Element Method," *Int. J. Heat Mass Transfer*, **27**, 815 (1984).

Brown, R. C., et al., "The Use of Wire Probes for the Measurement of Liquid Film Thickness in Annular Gas-Liquid Flows," *Can. J. Chem. Eng.*, **56**, 754 (1978).

Dukler, A. E., "Characterization, Effects and Modelling of the Wavy Gas-Liquid Interface," *Prog. Heat Mass Transfer*, **6**, 207 (1972).

———, "The Role of Waves in Two Phase Flow: Some New Understanding," *Chem. Eng. Educ., 1976 Award Lecture*, 108 (1977).

Gosman, A. D., et al., *Heat and Mass Transfer in Recirculating Fluid Flow*, Academic Press, London (1969).

Hanratty, T. J., and J. A. Campbell, "Measurement of Wall Shear Stress," *Fluid Mechanics Measurements*, R. J. Goldstein, ed., Hemisphere, Washington, DC, 559 (1983).

Huang, P. G., et al., "Discretization of Nonlinear Convection Processes: A Broad-Range Comparison of Four Schemes," *Comp. Meth. Appl. Mech. Eng.*, **48**, 1 (1985).

Kapitza, P. L., "Wave Flow of Thin Layers of a Viscous Fluid," *Collected Papers of P. L. Kapitza*, **II**, Macmillan, New York (1964).

Kheshgi, H. S., and L. E. Scriven, "Disturbed Film Flow on a Vertical Plate," *Phy. Fluids*, **30**, 990 (1987).

Leonard, B. P., "A Stable and Accurate Convective Modelling Procedure Based on Quadratic Upstream Interpolation," *Comp. Meth. Appl. Mech. Eng.*, **12**, 59 (1979).

Levich, V. G., *Physiochemical Hydrodynamics*, Prentice-Hall, New York, 692 (1962).

Mao, Z.-X., and T. J. Hanratty, "The Use of Scalar Transport Probes to Measure Wall Shear Stress in a Flow with Imposed Oscillations," *Exp. Fluids*, **3**, 129, (1985).

Maron, D. M., et al., "Interfacial Structure of Thin Falling Films: Piecewise Modeling of the Waves," *Physico-Chem. Hydrodynam.*, **6**, 87 (1985).

Patankar, S. V., *Numerical Heat Transfer and Fluid Flow*, Hemisphere, Washington, DC, (1980).

Pollard A., and A. L. W. Siu, "The Calculation of Some Laminar Flows Using Various Discretization Schemes," *Comp. Meth. Appl. Mech. Eng.*, **35**, 293 (1982).

Raithby, G. D., "A Critical Evaluation of Upstream Differencing Applied to Problems Involving Fluid Flow," *Comp. Meth. Appl. Mech. Eng.*, **9**, 75 (1976).

Zabaras, G. J., "Studies of Vertical, Annular Gas-Liquid Flow," Ph.D. Diss., Univ. Houston (1985).

Zabaras, G. J., et al., "Vertical Upward Cocurrent Gas-Liquid Annular Flow," *AIChE J*, **32** (5), 829 (May, 1986).

Manuscript received May 9, 1988, and revision received Aug. 23, 1988.